Oncology and Translational Medicine
DOI 10.1007/s10330-022-0586-6
October 2022, Vol. 8, No. 5, P239–P246

ORIGINAL ARTICLE

Allosteric probe-modified liposome loading bufalin-fluorouracil complex for targeted colorectal cancer therapy*

Fajiang Mao[1, 2], Xingli Wu[1], Chenyue Yuan[1], Haiyan Huang[1], Yanyan Qiu[1], Jianlin Ren[1] (✉), PeihaoYin[2] (✉)

[1] Department of Oncology, Shanghai Municipal Hospital of Traditional Chinese Medicine, Shanghai University of Traditional Chinese Medicine, Shanghai 200071, China
[2] Interventional Cancer Institute of Chinese Integrative Medicine, Putuo Hospital, Shanghai University of Traditional Chinese Medicine, Shanghai 200062, China

Abstract

Objective Bufalin, the main active anti-tumor monomer of toad venom, is crucial in cancer treatment. However, intrinsic issues, such as poor solubility and systematic toxicity, have considerably mitigated its anticancer functions and caused unwanted side effects. It is essential to develop innovative targeting systems to precisely and efficiently deliver anticancer drugs to achieve satisfying therapeutic efficiency.

Methods This work established a novel and more efficient system for simultaneously detecting and killing colorectal cancer cells. The proposed method designed two allosteric probes, a report probe and a recognize probe. The method exhibited high sensitivity towards cell detection via the recognizing probe identifying target cancer cells and the report probe's signal report. Combining bufalin and fluorouracil endowed better tumor cell inhibition.

Results We observed significantly enhanced fluorescence dots surrounding the HCT-116 cell membranes. No fluorescence increments in the other three cells were identified, indicating that the established liposome complex could specifically bind with target cells. In addition, the best ratio of bufalin to fluorouracil was 0.15 and 0.5, respectively. This improved the anti-tumor effects and achieved more than 60% tumor cell inhibition.

Conclusion This method will provide new opportunities for intracellular biomolecule detection and targeted cancer cell therapy.

Received: 30 June 2022
Revised: 21 July 2022
Accepted: 26 August 2022

Key words: bufalin; fluorouracil; colorectal cancer; imaging; therapy

Globally, colorectal cancer (CRC) is one of the most threatening malignant tumors, the second most common cancer, and the second leading cause of death. It seriously affects patients' life quality and brings heavy economic burden to the society [1-3]. In recent years, CRC incidence and mortality have increased due to gradually deteriorating factors, such as environment, occupation, living habits, and inheritance [4, 5]. CRC incidence has been rapidly rising in those under the age of 50 over the last 20 years [6]. Therefore, it is vital to establish complete novel nanomaterials with high tumor accumulation to deliver therapeutic units that augment therapeutic efficiency.

Bufalin is the main active anti-tumor monomer of toad venom, a kind of traditional Chinese medicine secreted from the glands behind the ears of *Bufo gargarizans* [7-9]. Bufalin has therapeutic effects on various solid tumors, including gastric cancer, liver cancer, esophageal cancer, lung cancer, and leukemia, due to its characteristics, such as inducing tumor cell apoptosis, inhibiting tumor cell proliferation, inhibiting tumor blood vessel formation,

✉ Correspondence to: Peihao Yin. Email: yinpeihao@shutcm.edu.cn
Jianlin Ren. Email: renjianlin666@126.com
* Supported by grants from the Medical Guidance Project of Shanghai Science and Technology Commission (No. 19401935200) and the Budget Internal Medicine Research Project of Shanghai University of Traditional Chinese Medicine (No. 2020LK065).

reversing tumor cell multidrug resistance, and promoting or enhancing tumor cell differentiation [10, 11]. Even though numerous studies have proven bufalin's potential anti-tumor influence, it is also criticized for cardiac side effects, such as arrhythmia and conduction block, limiting its clinical application [10, 12]. Additionally, the characteristics of bufalin, such as its insolubility in water, fast metabolism, and short half-life in the body, greatly limit its application in cancer treatment [13, 14]. Scientists have strived to deal with these deficiencies and promote applying bufalin in tumor therapy. Currently, there are two main methods for improving the performance of bufalin: chemically modifying the bufalin structure to create bufalin derivatives or circumventing its shortcomings through nanotechnology. For example, Zou *et al.* [15] embedded bufalin in the cavity of β-cyclodextrin (β-CD) to obtain higher stability and anti-tumor effects. They demonstrated that the water solubility of the complex was 24 or 34 times greater in water and phosphate-buffered saline (PBS) buffer, respectively. In recent years, various liposome-based methods to enhance the water solubility of bufalin have been proposed [16-18]. Li *et al.* [19] suggested a composed method that could realize the synergetic therapeutic efficacy of bufalin against melanomas by utilizing immune-liposome bufalin and anti-cluster of differentiation 40 (CD40) antibody adjuvant co-delivery. Although these methods have ameliorated the development of highly efficient bufalin-based strategies with better biocompatibility, their inability to simultaneously report tumor cells and therapeutic progress does not meet the requirements of accurate cancer therapies.

Herein, we proposed a novel and more efficient system for simultaneously detecting and killing CRC cells. We designed two allosteric probes: a report probe and a recognize probe. The recognize probe specially binds with the surface proteins of target cancer cells and release a blocker probe to initiate an attached rolling circle amplification (RCA) process. The recognize probe facilitates liposome and target cancer cell fusion, resulting in the transport of the report probe to the surface of the liposome and target cancer cells. Bufalin goes into cancer cells for anti-tumor treatment. In addition, RCA products induced by the released blocker probe unfold the report probes and generate fluorescence to flag the occurrence of the anti-tumor treatment.

Materials and methods

Materials

Liposome3000 (Lipofectamine® 3000 Transfection Reagent), the liposome extruder, and the filter membrane were provided by Invitrogen (Carlsbad, California, USA), Mercer (Shanghai, China), and Beyotime Biotechnology Co., Ltd. (Shanghai, China), respectively. Bufalin and 5-fluorouracil were purchased from Shanghai Ronghe Pharmaceutical Technology Development Co., Ltd. (Shanghai, China) and Beijing Soulebao Technology Co., Ltd. (Beijing, China), respectively.

We obtained HCT116 colon cancer cells, A549 lung cancer cells, HeLa cervical cancer cells, and FHC normal colon epithelial cell lines from the Shanghai Institute of Life Sciences, Chinese Academy of Sciences cell bank. All cells were cultured in Roswell Park Memorial Institute (RPMI)-1640 medium containing penicillin (100 U/mL) and streptomycin (100 g/mL) in 10% fetal bovine serum and placed in a 37 °C constant temperature and humidity incubator with 5% CO_2. Cells were sub-cultured every three days.

Table 1 details the oligonucleotide nucleic acids used in the experiment. The oligonucleotide nucleic acids used in this study were bought and purified from Shanghai Sangon Biological Engineering Technology and Services Co., Ltd. (Shanghai, China). The obtained oligonucleotide nucleic acids were diluted to 10 μM by high-performance liquid chromatography (HPLC) water and stored for the following experiments. The buffer-related regents and enzymes, such as bovine serum albumin (BSA), phi29 DNA polymerase, and T4 DNA ligase enzymes, were purchased from New England BioLabs (MA, USA). Fluorescence spectra were detected by a Hitachi F-4700 Fluorescence Spectrophotometer (Beijing, China). All solutions were prepared with ultrapure water, obtained using a water purification system (Milli-Q, Germany).

Methods

Investigating the designed allosteric probe for target cell recognition

We labeled the fluorescent probe and the corresponding quenching group on both ends of the allosteric probe. The purified and diluted allosteric probe was heated to 95 °C for 5 min and then slowly cooled to room temperature within 20 min. Afterward, 5 μL allosteric probe was mixed with the cells for 30 min. The fluorescence signals were detected using a Hitachi F-4700 Fluorescence Spectrophotometer (Beijing, China).

Table 1 Synthesized oligonucleotide sequence details

Title	Sequence (5'–3')
H1 probe	GAC GAC TAA TAA GAT TAA TCC TGT CCT CAA CAT CAG TCT GA TAA GCT AAT GTT CCT CAG CTG CTC TAG CTT ATC AGA CTG
H2 probe	TGT CCT AAT TAG AAT AAT CTC GAG TTC TAA GCT AGA GCA TC CAA TCA ACA TTA GCT TAT CAG ACT GAT GTT GAT TGG ATG CTC
S strand	AAC AGG ATT AAT CTT ATT AGT CGT CCT CGA GAT TAT TCT AAT TA GGA CAG CAG TTG AGG TAA TAG TCA CG

Detection performance evaluation

Obtained cells were diluted to different concentrations with RNase-free ddH_2O to investigate the detection sensitivity of the method. Different concentrations of cells (15 μL), 15 μL T4 DNA ligase enzyme, and 10 μL of established sensing scaffold were mixed in 4 μL 10× NE Buffer and incubated for 50 min at 37 °C. Afterward, the fluorescence spectra from 500 nm to 700 nm were collected in a 100 μL quartz cuvette with 490 nm excitation. We evaluated the method's selectivity by detecting different synthesized microRNAs (miRNAs) using the above procedures.

Establishing a subcutaneous transplanted tumor model in BALB/C nude mice

SPF grade BALB/C nude mice (20, four-week-old, male mice weighing 20 ± 2 g) were provided by the Shanghai SHREK company (License Number scxk 2017-0005) (Shanghai, China). They were raised and managed in the SPF-grade animal room of the Municipal Hospital of Traditional Chinese Medicine affiliated with the Shanghai University of Traditional Chinese Medicine. A 1-mL sterile syringe was used to aspirate cells with a density of 1×10^7/mL. The HCT116 cell suspension (100 μL) was injected when the needle reached the inoculation site. Then the nude mice were put back into the cage, and their general states were recorded. When the tumor body of nude mice grew to more than 62.5 cm^3, bufalin and 5-fluorouracil were encapsulated in liposomes modified with allosteric probes (the ratio of the two drugs was 0.15 μM bufalin to 12.5 μM 5-fluorouracil). We intraperitoneally injected 4.2 mg/kg of drug-loaded liposomes every two days, and the cumulative administration intervention lasted 30 days.

Live imaging observations of small animals

We injected 5 μL (10 μM) of allosteric probe-modified drug-loaded liposomes into the tumor site of the mice and observed the reaction for 30 min. The RCA product (5 μL) was injected into the tumor site. After 1 h, the nude mice were imaged. The fluorescence signal of the tumor body was detected by a small animal imager, and the excitation and emission lights were 530–550 and 560–600 nm, respectively (the fluorescent dye of the probe was Cy3. Its best excitation wavelength is 540 nm, and the emission wavelength is 570 nm).

Hematoxylin and eosin (HE) pathological staining

The nude mice were killed, subcutaneous tumor bodies were stripped, weighed, and measured, and the liver tissue and subcutaneous tumor of the nude mice were taken out for paraffin embedding. The specimens were clamped into the embedding box and put into the paraffin embedding machine for embedding. The wax blocks were put into the microtome for slicing 4 μM thick tissue paraffin sections. The wax block was put into a 60 °C oven and preheated for 10 min. Xylene, absolute ethanol, 95% ethanol, 80% ethanol, and 70% ethanol were dewaxed for 2 min. The following HE staining steps were executed:

i) Hematoxylin staining solution for 10 min.
ii) Differentiation solution for 30 s.
iii) Eosin staining solution for 2 min.
iv) Tap water washing and soaking for 5 min.
v) 95% ethanol and absolute ethanol dehydration for 2 min.
vi) Xylene permeabilization for 2 min.

The specimens were sealed with neutral gum and observed under an optical microscope (magnification: × 4 and × 40). According to the results of the pathological sections of liver tissues of nude mice in each group, all the groups showed liver damage except for the control group and group C, but no serious systemic adverse reactions occurred.

Data analysis

Each test underwent at least three independent replicates, displayed as the mean ± standard deviation (SD). Data were visualized using GraphPad Prism 8.0 software (CA, USA). A Student's *t*-test was used to analyze the comparisons between two groups. Multiple groups were compared with a one-way ANOVA and the least-significant difference (LDS) method. Differences were considered significant when $P < 0.05$.

Results

Working principle of the proposed strategy

Fig. 1 illustrates the working mechanism of the method. The proposed method for simultaneously detecting and treating CRC was mainly composed of two parts: i) fluorescence generation after the target CRC cells were recognized to report the occurrence of tumor cells and aptamer facilitated fusion of target colorectal cells with liposome, resulting in bufalin transport from liposomes to target cells to kill tumor cells. We designed two allosteric probes, the report and recognize probes (Fig. 1a), for the detection process. The recognize probe contained two DNA sequences: an aptamer sequence that could recognize the surface proteins of target cells and a blocker probe for initiating RCA. The report probe was designed with a hairpin structure and a cholesterol on its terminal to anchor it on the surface of liposomes and colorectal cells. We utilized liposomes to deliver bufalin and simultaneously improve water solubility for the anti-tumor process (Fig. 1b). The target cell protein aptamer in the designed recognize probe could provide targeted CRC cell recognition and accelerate liposome and colorectal cell fusion. The anti-tumor liposome complex was established by packaging bufalin with liposomes and loading the two designed allosteric probes onto the surface. In practice, the recognize probe on the surface of the liposome complex could bind with surface proteins

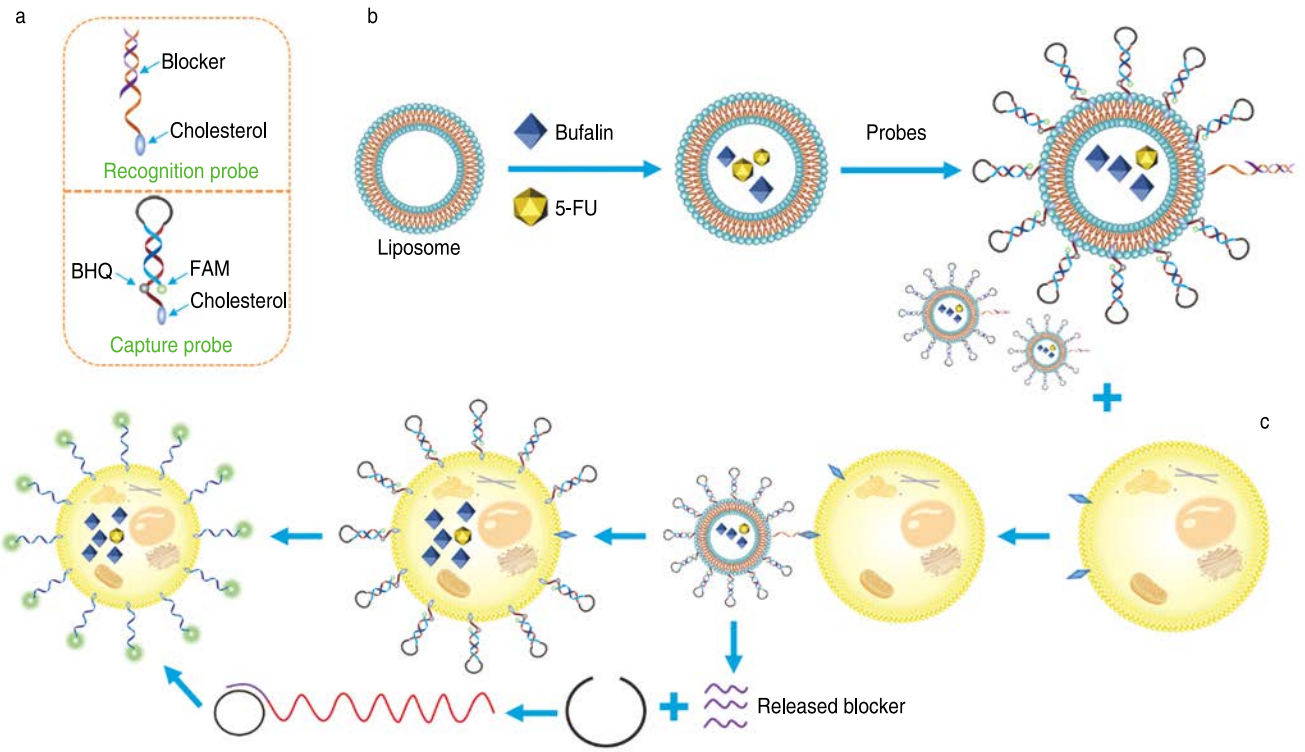

Fig. 1 The working principle of the proposed method for simultaneously detecting and therapizing CRC. (a) Details on how to design report and recognize probes; (b) Assembling bufalin into liposomes and the anchor designed allosteric probes on the liposome surface; (c) The working process of the method

by interacting with the aptamer and then draw them up when identifying the target CRC cells. Moreover, the aptamer-based recognition between the liposome complex and target CRC cells could facilitate liposomes fusing with cells and release blockers in the recognize probe. Meanwhile, the released blocker could further initiate the RCA process to produce single-strand DNA (ssDNA) sequences. As a result, the report probes on the surface of liposomes may be transported to the surface of target colorectal cells, importing bufalin into cancer cells to exert anti-tumor effects. Simultaneously, the obtained RCA products could recognize and specifically unfold report probes to generate fluorescence and flag tumor cells.

Investigating the designed probes and bufalin and 5-fluorouracil anti-tumor effects

The two probes were designed with different secondary structures with distinctive functional requirements. The recognition probe was composed of two parts, an aptamer of the cancer cell surface protein and a complementary blocker sequence. The report probe was designed with a stem-loop structure, which the RCA product could unfold to produce fluorescence. It is worth noting that the 3'-ends of these two probes were linked with cholesterol to anchor them in the phospholipid bilayer. First, we verified whether the designed recognition probe could specifically recognize target cancer cells and release the blocker sequences through a fluorescence assay (Fig. 2a). As shown in Fig. 2b, the obtained fluorescence intensity of the probes, when incubated with target CRC cells, was significantly higher than that in the control group. Furthermore, there were no obvious fluorescence enhancements in the non-specific group to incubate the probe with NCM 356 cells, which has no corresponding proteins on its surface, indicating that the designed recognize probe could specially bind with target cells and release blocker probes. We studied the RCA process through polyacrylamide gel electrophoresis (PAGE) analysis with a synthesized blocker as the initiator. We observed an approximately 20 bp band in lane 1 in the PAGE results. When the blocker was mixed with a padlock in lane 2, a higher band appeared (approximately 50 bp) – the complemented blocker and padlock complex. In lane 3, a light band was stuck in the well, indicating a long product that could not flow down (Fig. 2c). Therefore, the released blocker could hybridize with the two terminals of the padlock and subsequently initiate the RCA process. We then investigated whether the obtained RCA products could unfold the report probe through a fluorescence assay. As shown in Fig. 2d, we obtained an enhanced fluorescence when the RCA products were

mixed with the report probe. Furthermore, no significant fluorescence was observed when the report probe was incubated with other DNA sequences, demonstrating that the RCA products could specifically recognize and unfold the report probe to generate fluorescence signals.

We studied the anti-tumor effect of bufalin and 5-fluorouracil by detecting HCT116 cell viability after treating them with bufalin for different time periods. We concluded that bufalin and 5-fluorouracil could inhibit and kill HCT116 cells (Fig. 2c). 5-fluorouracil showed a relatively more stable inhibitory effect on cells. The inhibitory effect of both drugs was lower than 0.4, which is relatively low and needs further improvements (Fig. 2e). We decided to use bufalin in combination with 5-fluorouracil to increase the anti-tumor effect and optimize the ratio of bufalin to 5-fluorouracil. The results confirmed that the best ratio of bufalin to fluorouracil was 0.15 μM (bufalin) and 12.5 μM (fluorouracil), which could achieve more than a 60% tumor cell inhibition effect. Hence, combining the drugs showed better tumor cell inhibition (Fig. 2f).

Optimizing liposome complex assembly and the RCA process

The anti-tumor effect of the liposome complex loading bufalin and 5-fluorouracil may be closely associated with liposome size. Therefore, we investigated the anti-tumor effect of the liposomes with different sizes by detecting

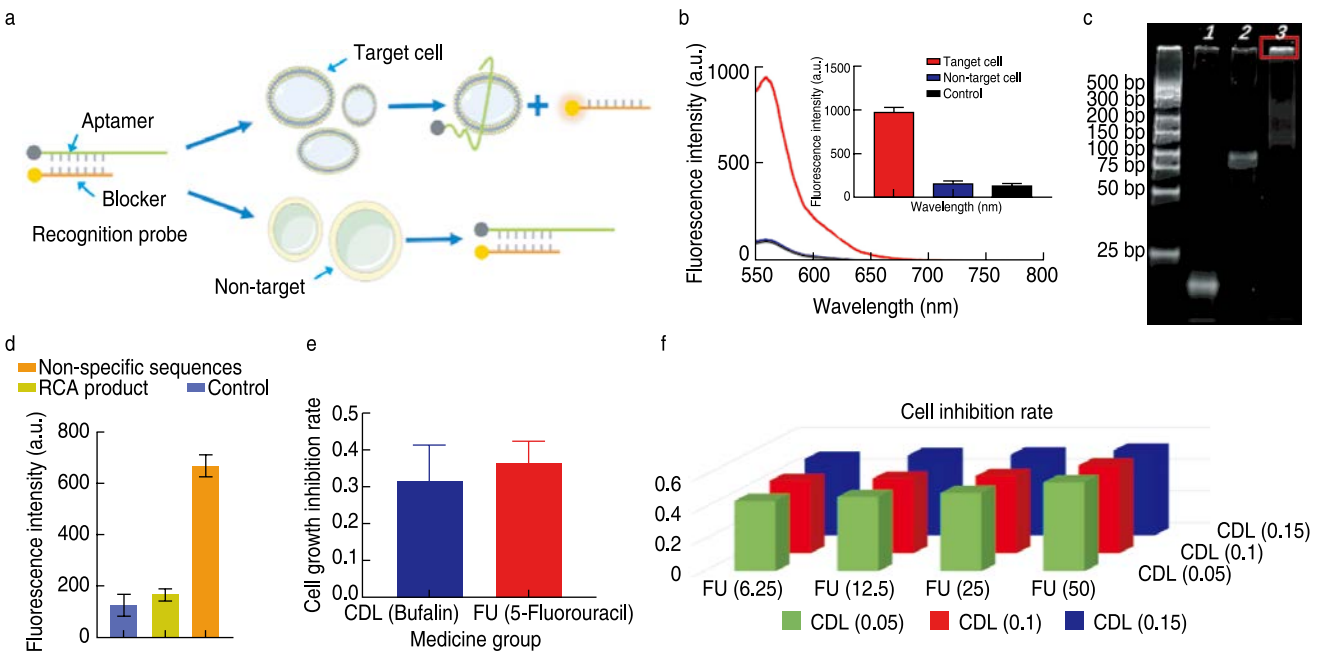

Fig. 2 Investigating the designed probes and bufalin and 5-fluorouracil anti-tumor effects. (a) Illustration of the fluorescence assay for investigating the recognition probe; (b) Fluorescence spectrum of the recognition probe when incubated with the target cell, non-specific cell, and control (1× PBS buffer); (c) PAGE analysis of the RCA process with a synthesized blocker as an initiator; (d) Fluorescence intensity report probes when incubated with RCA products or not; (e) HCT116 cell viability after liposome complex treatments; (f) Cell inhibition rate when treated with bufalin in combination with 5-fluorouracil at different ratios

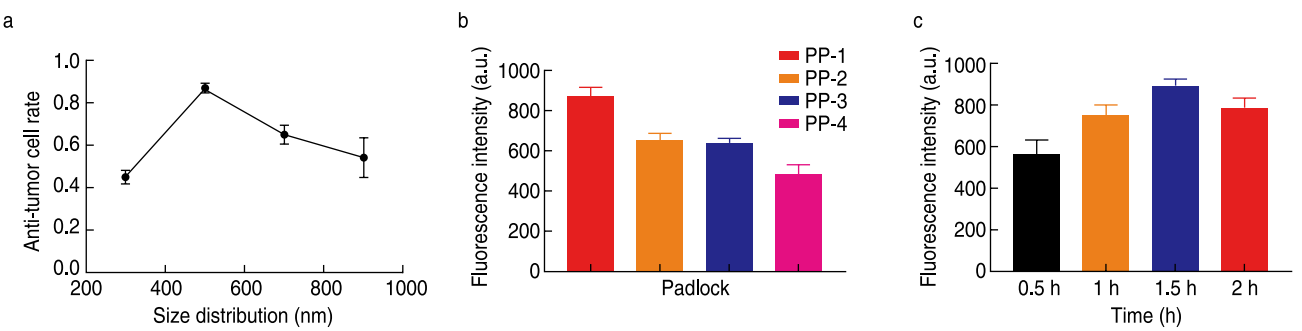

Fig. 3 Optimizing liposome complex assembly and the RCA process. (a) Anti-tumor cell rate of the liposome complex with different size distributions; (b) Fluorescence intensity of the RCA process with the four designed padlocks; (c) Fluorescence intensity of the RCA process at different times

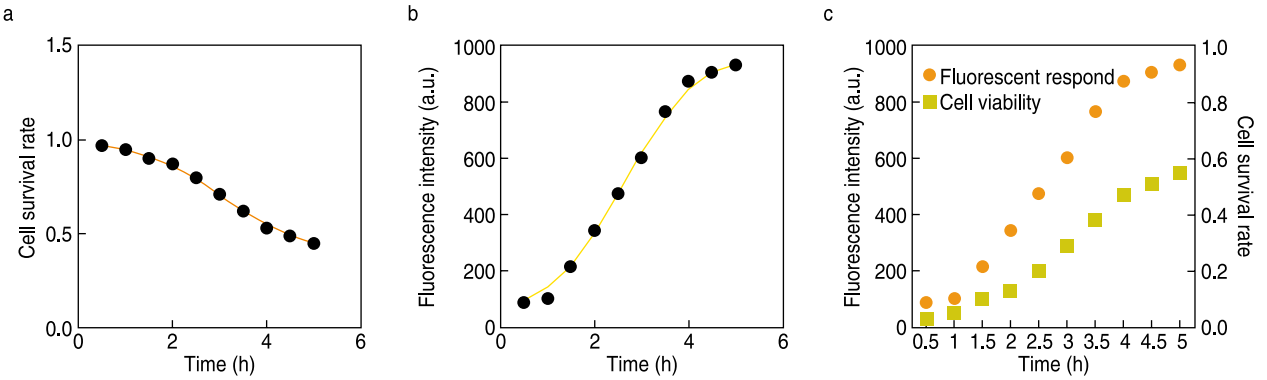

Fig. 4 The proposed method inhibits CRC *in vitro*. (a) HCT116 cell viability was obtained at different incubation times; (b) HCT116 cell fluorescence intensities were obtained at different incubation times; (c) Comparison of tumor inhibition rate and fluorescence intensity over time

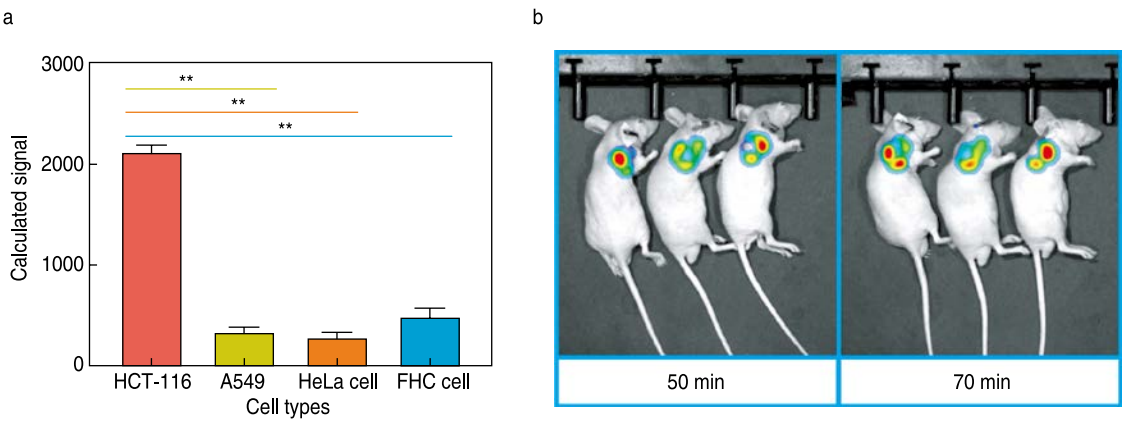

Fig. 5 Analytical performance of the proposed method. (a) Fluorescence signal of the cell when incubated with the established biosensor; (b) Animal imaging of the constructed CRCs after 50 min and 70 min of incubation

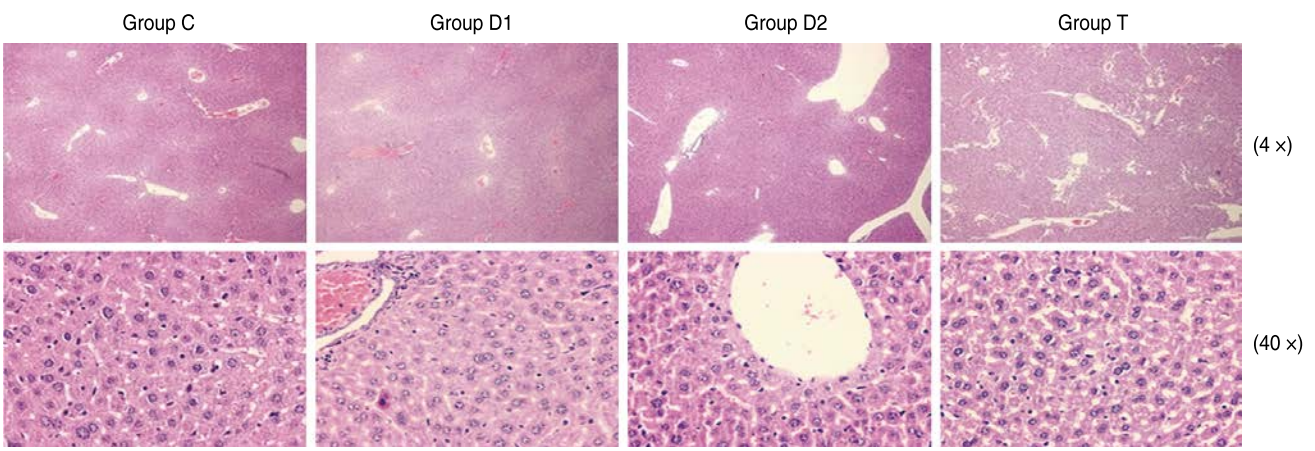

Fig. 6 Comparison of HE staining in the livers of nude mice in each group

cell viability after incubating them with HCT116 cells. The anti-HCT116 cell rate increased with liposome size, ranging from 300 nm to 500 nm (Fig. 3a). No further enhancements were observed with sizes greater than 500 nm, suggesting that liposomes with a 500 nm diameter could provide an optimized anti-tumor effect. Hence, we designed a desired padlock that could not be cyclized by undesired DNA sequences (PP1, PP2, PP3, and PP4)

with varied complementary lengths and blocker and secondary structures to meet such a requirement (Table S1). The fluorescence assay showed that all four padlocks initiated the RCA reaction in the presence of the blocker (Fig. 3b). PP1 had a length of 42 nucleotides, no inner hairpin structure, and yielded the highest fluorescence intensity. We investigated the time of the RCA process and observed the most RCA products at 1.5 h (Fig. 3c), indicating that the time for RCA is also enough for liposomes and cancer cells to fuse.

Feasibility of the proposed method for CRC treatments in vitro

We tested the cell viability of HCT116 cells treated with the complex at various intervals to confirm the anti-tumor efficacy of the liposome complex loading bufalin and 5-fluorouracil in CRC cells. We found that the anti-tumor effect of this complex was time-dependent (Fig. 4a). In addition, we showed that the fluorescence intensity increased over time and was positively correlated with impaired tumor growth (Fig. 4b, c). In summary, these data revealed the anti-tumor effects of the complex in vitro and its time and dose dependence.

Feasibility of the proposed method for CRC treatments in vivo

With the HCT116 cells as the target, we tested the fluorescence response of the system after recognizing the target CRC cells under the optimized experimental conditions. As illustrated in Fig. 5a, we applied the whole sensing system to detect HCT116 cells and three other cells that did not express the corresponding proteins on their membrane surfaces. We eventually noticed significantly enhanced fluorescence dots surrounding HCT116 cell membranes and no fluorescence increments in the other three cells, indicating that the established liposome complex could specifically bind with target cells. Having demonstrated the *in vitro* sensing capability of the established liposome complex, we sought to test its performance in *in situ* imaging and targeted therapy in a xenograft mouse model. A CRC model was utilized to investigate targeted identification and therapy. The fluorescence signal of the cancer models was monitored with different incubation times to uncover whether target protein recognition could specifically induce the following *in situ* imaging process and facilitate cell fusion. The fluorescence signal of liposome-treated cancer models dramatically increased when incubated for 60 min, while the control groups (without adding the liposome complex) displayed minimal tumor fluorescence enhancement (Fig. 5b).

In addition, we found that this liposome complex had no severe systemic side effects in the HE-stained liver and spleen tissues of mice treated with this complex or the corresponding control. We then evaluated therapeutic safety by analyzing the collected main viscera. We also collected normal organs of control mice (no tumor inoculation) under the same condition to reasonably evaluate possible side effects and other significant differences. Firstly, we investigated possible hepatic toxicity. According to the HE pathological sections of liver tissues of nude mice in each group, except for the control group, all groups showed slight liver damage, but no serious systemic adverse reactions occurred (Fig. 6).

Conclusion

This study established novel nuclear-shell biopolymers by loading bufalin and 5-fluorouracil into liposomes and anchoring the designed recognition and report probes. After recognizing the target CRC cell, the released blocker initiated the RCA process and unfolded the report probes. This strategy will aid in specific cancer cell recognition and reduce the undesired death of healthy cells that commonly occurs in conventional chemotherapy. This method will provide new opportunities for intracellular biomolecule detection and targeted cancer therapy.

Acknowledgments

Not applicable.

Funding

Supported by grants from the Medical Guidance Project of Shanghai Science and Technology Commission (No. 19401935200) and the Budget Internal Medicine Research Project of Shanghai University of Traditional Chinese Medicine (No. 2020LK065).

Conflicts of interest

The authors indicated no potential conflicts of interest.

Author contributions

All authors contributed to the data acquisition and interpretation and reviewed and approved the final version of this manuscript.

Data availability statement

Not applicable.

Ethical approval

This study was approved by the Experimental Animal Ethics Committee of Shanghai Municipal Hospital of Traditional Chinese Medicine, Shanghai University of Traditional Chinese Medicine.

References

1. Kishore C, Bhadra P. Current advancements and future perspectives of immunotherapy in colorectal cancer research. Eur J Pharmacol.

2021 Feb 15;893:173819.
2. Rajendran S, Barbon S, Pucciarelli S. Spotlight on circadian genes and colorectal cancer crosstalk. Endocr Metab Immune Disord Drug Targets. 2021;21(1):4-11.
3. Harlé A. Cell-free DNA in the management of colorectal cancer. Recent Results Cancer Res. 2020;215:253-261.
4. Perrod G, Rahmi G, Cellier C. Colorectal cancer screening in Lynch syndrome: Indication, techniques and future perspectives. Dig Endosc. 2021;33(4):520-528.
5. Patel SG, Murphy CC, Lieu CH, et al. Early age onset colorectal cancer. Adv Cancer Res. 2021;151:1-37.
6. Patel SG, Ahnen DJ. Colorectal cancer in the Young. Curr Gastroenterol Rep. 2018;20(4):15.
7. Cho YJ, Lee JE, Park MJ, et al. Bufalin suppresses endometriosis progression by inducing pyroptosis and apoptosis. J Endocrinol. 2018;237(3):255-269.
8. Lan YL, Wang X, Lou JC, et al. Bufalin inhibits glioblastoma growth by promoting proteasomal degradation of the Na+/K+-ATPase α1 subunit. Biomed Pharmacother. 2018;103:204-215.
9. LingHu HR, Luo H, Gang L. Bufalin induces glioma cell death by apoptosis or necroptosis. Onco Targets Ther. 2020;13:4767-4778.
10. Lan YL, Lou JC, Jiang XW, et al. A research update on the anticancer effects of bufalin and its derivatives. Oncol Lett. 2019;17(4):3635-3640.
11. Xie Y, Yan X, Sun L. The mechanism of bufalin-induced apoptosis of K562/A02. Med Sci Monit. 2019;25:2542-2552.
12. Li M, Wang XJ, Zhao Q, et al. Bufalin-induced cardiotoxicity: new findings into mechanisms. Chin J Nat Med. 2020;18(7):550-560.
13. Cheng CS, Wang J, Chen J, et al. New therapeutic aspects of steroidal cardiac glycosides: the anticancer properties of Huachansu and its main active constituent Bufalin. Cancer Cell Int. 2019;19:92.
14. Emam H, Refaat A, Jawaid P, et al. Hyperthermia and radiation reduce the toxic side-effects of bufadienolides for cancer therapy. Oncol Lett. 2017;14(1):1035-1040.
15. Zou A, Zhao X, Handge UA, et al. Folate receptor targeted bufalin/β-cyclodextrin supramolecular inclusion complex for enhanced solubility and anti-tumor efficiency of bufalin. Mater Sci Eng C Mater Biol Appl. 2017 Sep 1;78:609-618.
16. Yuan J, Zeng C, Cao W, et al. Bufalin-loaded PEGylated liposomes: antitumor efficacy, acute toxicity, and tissue distribution. Nanoscale Res Lett. 2019;14(1):223.
17. Yuan J, Zhou X, Cao W, et al. Improved antitumor efficacy and pharmacokinetics of Bufalin via PEGylated liposomes. Nanoscale Res Lett. 2017;12(1):585.
18. Gao L, Zhang L, He F, et al. Surfactant assisted rapid-release liposomal strategies enhance the antitumor efficiency of bufalin derivative and reduce cardiotoxicity. Int J Nanomedicine. 2021;16:3581-3598.
19. Li Y, Yuan J, Yang Q, et al. Immunoliposome co-delivery of bufalin and anti-CD40 antibody adjuvant induces synergetic therapeutic efficacy against melanoma. Int J Nanomedicine. 2014;9:5683-5700.

DOI 10.1007/s10330-022-0586-6
Cite this article as: Mao FJ, Wu XL, Yuan CY, et al. Allosteric probe-modified liposome loading bufalin-fluorouracil complex for targeted colorectal cancer therapy. Oncol Transl Med. 2022;8(5):239–246.